De-noising of two-dimensional angular correlation of positron annihilation radiation data using Daubechies wavelet thresholding

1997 J. Phys.: Condens. Matter 9 10293

(http://iopscience.iop.org/0953-8984/9/46/026)

J. Phys.: Condens. Matter **9** (1997) 10293–10299. Printed in the UK PII: S0953-8984(97)85727-X

De-noising of two-dimensional angular correlation of positron annihilation radiation data using Daubechies wavelet thresholding

A G Major†, H M Fretwell†, S B Dugdale‡, A Rodriguez-González† and M A Alam†

† H H Wills Physics Laboratory, University of Bristol, Tyndall Avenue, Bristol, BS8 1TL, UK

‡ Université de Genève, Département de Physique de la Matière Condensée, 24 quai Ernest Ansermet, CH-1211 Genève 4, Switzerland

Received 7 July 1997

Abstract. Two-dimensional **a**ngular **c**orrelation of positron **a**nnihilation **r**adiation (2D-ACAR) experiments provide a means of determining the electron–positron momentum density in metals and alloys over a wide range of temperatures. A difficult task regarding this method is the reconstruction of the three-dimensional density from a limited number of two-dimensional projections. Difficulties arise from noise superimposed on the data. This paper explains and demonstrates the use of a *wavelet* noise filter, and gives a comparison of wavelet and Fourier filters.

1. Introduction

The analysis of experimental data is often based on the linear expansion of the measured data in complete and orthogonal function bases. Such an expansion (or transform, synonymously) into a different domain can be useful for filtering data and/or extracting information. As an example, the Fourier expansion using basis functions of the form e^{ikx} yields direct information about wavenumber and phase, while losing any spatial information.

In two-dimensional angular correlation of positron annihilation radiation (2D-ACAR) experiments, 2D projections of the electron–positron momentum density of a solid are measured [1]. The 3D density must be reconstructed from these projections. A reconstruction scheme proposed by Cormack for x-ray tomography [2, 3] and later adapted for 2D-ACAR by Kontrym-Sznajd [4] has proved adequate for retrieving high-resolution three-dimensional distributions from 2D-ACAR data. The adaptation was necessary due to the limited number of projections (typically five) in 2D-ACAR experiments, as opposed to x-ray tomography. Although the algorithm yields realistic results, it introduces features in some reconstructions which cannot be inferred from the projections. This work shows that a simple *wavelet* noise reduction filter can efficiently reduce the appearance of these artefacts.

2. Wavelet expansion

2.1. Basic concepts

A novel area of applied mathematics is the variety of *wavelet* expansions [5, 6]. A one-dimensional wavelet basis is a set of functions $\Psi_{j,k}$ obeying

$$\Psi_{j,k}(x) = 2^{j/2}\Psi_{0,0}(2^j x - k) \tag{1}$$

0953-8984/97/4610293+07$19.50

$$\Psi_{0,0}(x) = \sqrt{2} \sum_{l=-\infty}^{\infty} v_l \varphi(2x - l) \tag{2}$$

$$\varphi(x) = \sqrt{2} \sum_{l=-\infty}^{\infty} u_l \varphi(2x - l) \tag{3}$$

where j, k, and l are integers, u_l and v_l are complex coefficients, and $\varphi(x)$ is the so-called scaling function. The coefficients u_l and v_l determine the properties of the wavelet basis. $\varphi(x)$ is given by u_l and v_l through (3), although it is not practically obtained in this way. Any well-behaved function $f(x)$ can then be expanded as

$$f(x) = \sum_{j,k} w_{j,k} \Psi_{j,k}(x) \tag{4}$$

where $w_{j,k}$ are the coefficients representing f in the wavelet domain. If the $\Psi_{j,k}$ are orthonormal, the $w_{j,k}$ are given by

$$w_{j,k} = \int_{-\infty}^{\infty} \overline{\Psi_{j,k}(x)} f(x) \, \mathrm{d}x \tag{5}$$

where the bar denotes complex conjugation.

In the particular case of the *real Daubechies class n wavelets* (n even) [6], the coefficients u_l and v_l are real, and only n of each are non-zero. The values of these elements are given by orthonormality of the $\Psi_{j,k}$ and by the conditions

$$\int_{-\infty}^{\infty} x^i \Psi_{j,k}(x) \, \mathrm{d}x = 0 \qquad i = 0, 1, \ldots, \frac{n}{2} - 1. \tag{6}$$

The Daubechies coefficients u_l and v_l and thus the wavelet basis are fully determined by equation (6) and the orthonormality conditions.

The wavelet basis functions (often referred to as wavelets) are generally localized in *both* real and wavenumber space. Figure 1 shows selected Daubechies wavelets in real space, visualizing their localization. The Daubechies wavelets even exhibit compact support in real space, which means that $\Psi_{j,k}(x)$ is zero outside a finite interval in x. The localization makes it possible to approximate most well-behaved functions with high accuracy as a linear combination of a small number of wavelets.

Another significant difference between the wavelets and conventional bases is the fact that the wavelets within a basis are derived from the others by shifting ($x \to x - k$) and scaling ($x \to 2^j x$), according to (1). This indirectly implies that *two* indices, j (scale) and k (position) are required to identify a wavelet, as opposed to a *single* parameter in conventional bases (e.g. the wavenumber in the Fourier case).

2.2. Discrete wavelet transforms

On one hand, the definition of wavelets in (1)–(3) appears to be impractical for numerical calculations. On the other hand, a corresponding discrete transform can be defined in analogy with the discrete Fourier transform. This involves matrix multiplications, the matrices being usually highly sparse and easily computable given the coefficients u_l and v_l. The knowledge of the scaling function $\varphi(x)$ is not required for the discrete transform. In the Daubechies case, the implementation is in fact easier than in the case of the Fourier transform [7]. The sample wavelets in figure 1 were calculated using the inverse discrete wavelet transform.

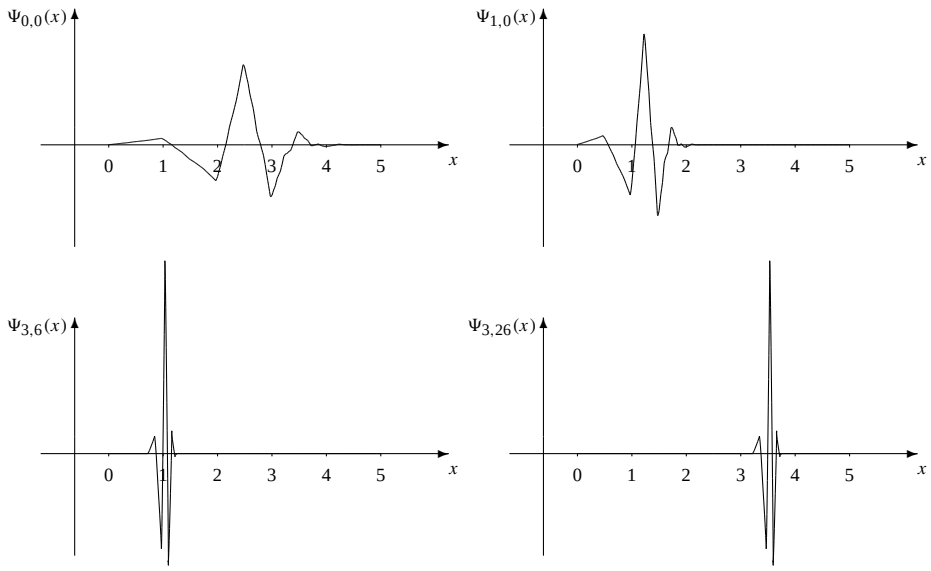

Figure 1. One-dimensional real Daubechies class 6 wavelets. The integer indices for scaling (j) and shifting (k) range from $-\infty$ to ∞ in order to make the wavelet basis complete.

2.3. Multi-dimensional wavelets

Like any other one-dimensional expansion, the wavelet expansion can be extended to functions of arbitrary dimension N by defining the basis functions as a product of the one-dimensional basis functions:

$$\Psi^{(N)}_{j_1,k_1,\ldots,j_N,k_N}(x_1,\ldots,x_N) = \prod_{i=1}^{N} \Psi^{(1)}_{j_i,k_i}(x_i). \tag{7}$$

Numerically, the transform can be reduced to subsequent one-dimensional transforms, thus allowing straightforward implementation.

3. De-noising

Conventional methods for data de-noising, such as Fourier filters, essentially blur the data while removing noise. This is partially a consequence of the de-localization of the basis functions. Due to their localization both in real and wavenumber space, wavelets can be efficiently used for de-noising without blurring the useful part of the data [8]. Therefore, even a simple algorithm can lead to significantly lower noise while leaving the resolution unchanged:

(i) transform the data into the wavelet domain;

(ii) set those elements in the wavelet domain to zero whose absolute values are smaller than a certain threshold;

(iii) transform the modified wavelet-domain data back to the real domain.

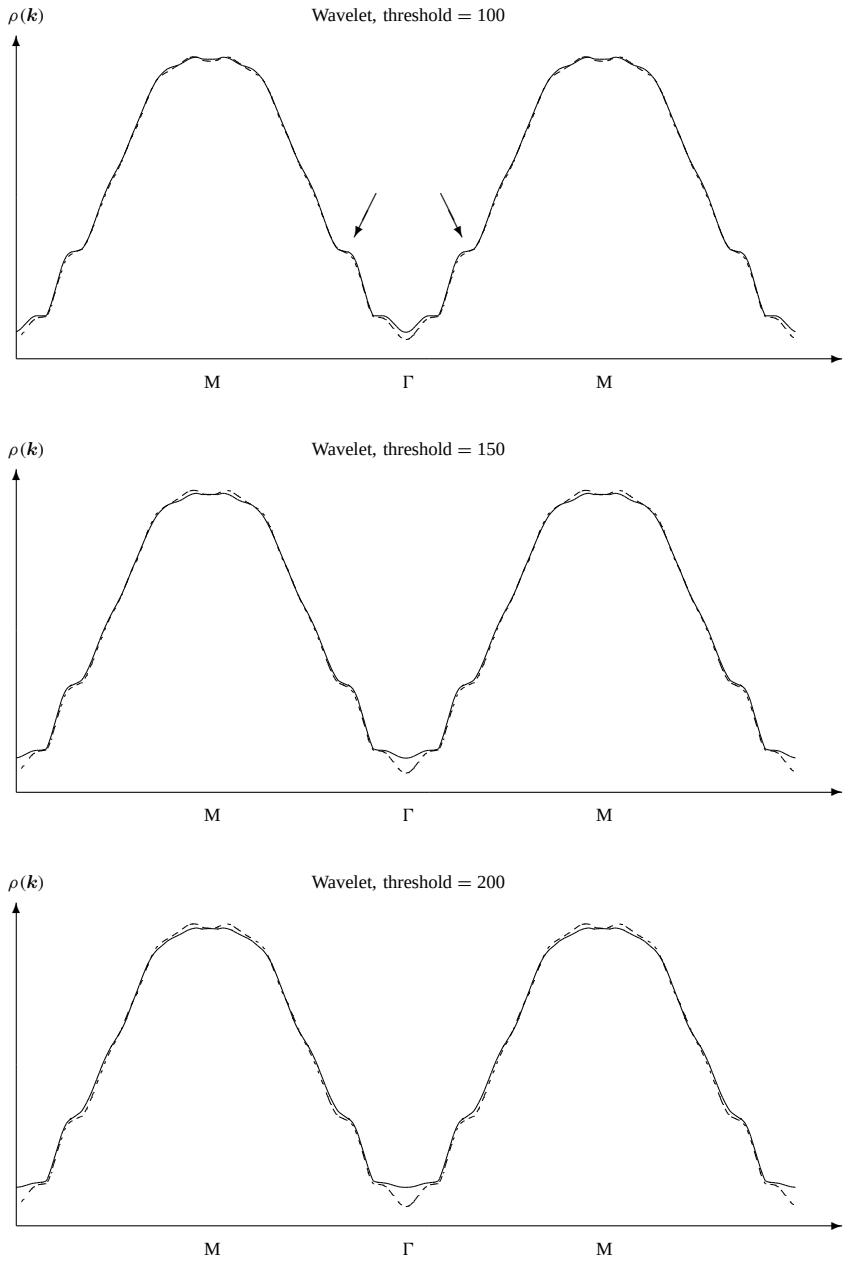

Figure 2. Cross-sections along the M–Γ–M direction through the reconstructed electron–positron momentum density $\rho(\boldsymbol{k})$ of a GdY alloy. The broken line shows the reconstruction from the original 2D-ACAR data. The full lines were obtained by reconstructing after processing through the Daubechies class 6 wavelet filter. The arrows indicate the important feature whose sharpness should be retained.

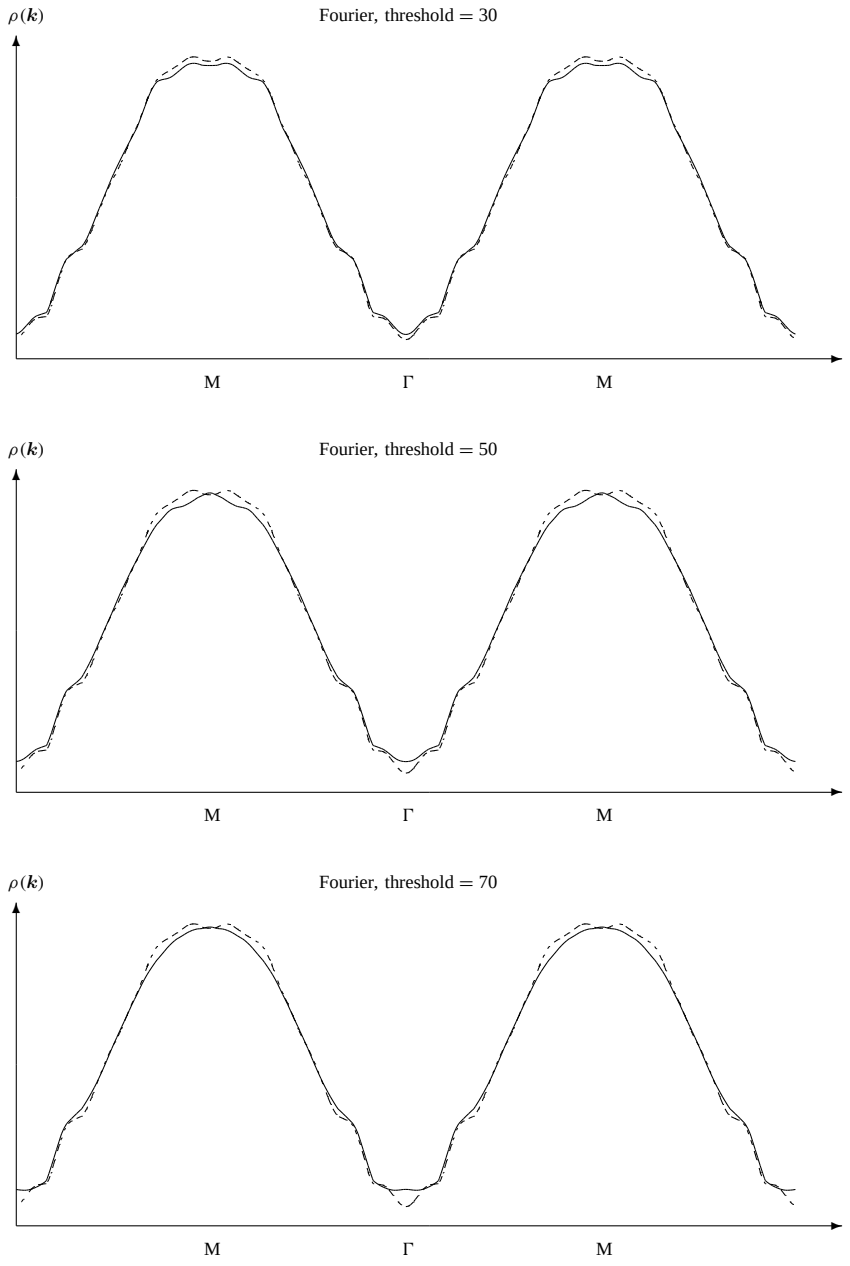

Figure 3. Cross-sections along the M–Γ–M direction through the reconstructed electron–positron momentum density $\rho(\boldsymbol{k})$ of a GdY alloy. The broken line shows the reconstruction from the original 2D-ACAR data. The full lines were obtained by reconstructing after processing through the Fourier filter.

The efficiency of this method was tested, using the Daubechies class 6 wavelet transform. Five projections obtained from 2D-ACAR measurements of a $Gd_{70}Y_{30}$ alloy at ≈50 K were filtered using this wavelet thresholding, prior to reconstruction using the Cormack method. The effect of the filter is shown in figure 2. The steps indicated by the arrows separate two sheets of the Fermi surface from each other—their sharpness should be retained by the filter—whereas the 'bumps' around the M and the Γ points are believed to be a consequence of noise. In fact these bumps disappear if one reduces the number of terms in the polynomial expansion used to describe the electron–positron momentum density, thus lowering the overall resolution of the reconstruction technique and its sensitivity towards noise.

As demonstrated in figure 2, the wavelet filter is capable of removing the unwanted features in the reconstruction without smoothing the important details. As the threshold is increased, the amplitude of the noise-related 'bumps' is decreased considerably before the sharpness of the steps separating the Fermi edges is affected. In the present case the ratio of cancelled wavelet coefficients varies between 95% and 99%, according to the threshold.

4. Comparison with Fourier de-noising

An analogous thresholding algorithm can be implemented using the Fourier transform instead of the wavelet transform. Figure 3 shows the results of such a filter, for comparison with figure 2. Again, equal thresholds were used for all projections, and the numbers of cancelled coefficients were similar to those for the corresponding wavelet case. Figures 2 and 3 demonstrate that the Fourier filter inevitably smooths the important features while removing the noise-related ones. Unlike in the case of the wavelet filter, efficient removal of noise cannot be combined with sufficient resolution. Furthermore, the value of the threshold is critical in the Fourier case. A slight change in the threshold can result in a significant change in the appearance of the artefacts. A smooth, monotonic variation of their amplitudes with the threshold value like that in the wavelet case cannot be observed.

5. Results

As the present investigation has shown, there are two significant differences between the behaviours of the wavelet and the Fourier filters.

(i) The blurring of the data: a measure of the resolution is the sharpness of the 'step' in the density between the Γ and M points. This step is a vital part of the electron–positron momentum density and should remain sharp. Figures 2 and 3 show that the Fourier method lowers the resolution to a larger extent than the wavelet method.

(ii) Predictability: the wavelet filter is more predictable than the Fourier filter. In the wavelet case, the effect of thresholding varies monotonically with the threshold. The threshold is more critical in the Fourier method.

The wavelet filter seems to remove noise efficiently. In 2D-ACAR in particular, it offers the possibility of detecting and removing unreal features in the reconstructed electron–positron momentum density.

Acknowledgments

One of the authors (AGM) wishes to express his thanks to the Studienstiftung des deutschen Volkes eV, Germany, and the Nuffield Foundation, UK, for financial support. Generous financial support from the EPSRC, UK, is also gratefully acknowledged.

References

[1] Berko S 1979 *Proc. 5th Int. Conf. on Positron Annihilation (ICPA-5)* ed R R Hasiguti and K Fujiwara (Sendai: Japanese Institute of Metals) p 65
[2] Cormack A M 1963 *J. Appl. Phys.* **34** 2722
[3] Cormack A M 1964 *J. Appl. Phys.* **35** 2908
[4] Kontrym-Sznajd G 1989 *Solid State Commun.* **70** 1011
[5] Walker J S 1997 *Not. Am. Math. Soc.* **44** 658
[6] Daubechies I 1988 *Comment. Pure Appl. Math.* **41** 909
[7] Press W H, Teukolsky S A, Vetterling W T and Flannery B P 1992 *Numerical Recipes in C* 2nd edn (Oxford: Oxford University Press)
[8] Donoho D L 1993 *Proc. Symp. Appl. Math.* **47** 173